

ARTICLE

Slow magnetic relaxation in dinuclear dysprosium and holmium phenoxide bridged complexes: a Dy_2 single molecule magnet with a high energy barrier

Received 00th January 20xx,
Accepted 00th January 20xx

DOI: 10.1039/x0xx00000x

Matilde Fondo,^{a,*} Julio Corredoira-Vázquez,^a Ana M. García-Deibe,^a Jesús Sanmartín-Matalobos,^a Silvia Gómez-Coca,^b Eliseo Ruiz^b and Enrique Colacio^c

Dinuclear $[M(H_3L^{1,2,4})_2]$ ($M = Dy, Dy_2; M = Ho, Ho_2$) complexes were isolated from an heptadentate aminophenol ligand. The crystal structures of $Dy_2 \cdot 2THF$, and the pyridine adducts $Dy_2 \cdot 2Py$ and $Ho_2 \cdot 2Py$, show that the complexes are dinuclear, with unsupported double phenoxide bridges, and that the N_4O_4 environment of the Ln^{III} centres is distorted triangular dodecahedral. The magnetic analysis of Dy_2 and Ho_2 shows that Dy_2 is a single molecular magnet (SMM), with a thermal-activated zero-field effective energy barrier (U_{eff}) of 367.7 K, the largest barrier shown by double phenoxide-bridged dinuclear dysprosium complexes to date. Ho_2 is one of the scarce dinuclear complexes showing frequency-dependence for the out-of-phase component of susceptibility, although it does not even show field-induced SMM behaviour above 2 K. *Ab initio* calculations were done in order to shed light on the magnetic dynamics of the complexes, and these studies support the experimental magnetic results.

Introduction

Lanthanoid(III) ions are the most promising candidates for constructing single-molecule magnets (SMMs) with high anisotropy energy barrier (U_{eff}) and blocking temperature (T_B).^{1–9} This is mainly due to the generally large magnetic moment, and huge magnetic anisotropy in lanthanoid ions. Accordingly, in recent years, the search for SMMs with high T_B has been directed toward lanthanoid compounds with a single paramagnetic metal centre, i.e., toward the so-called single ion magnets (SIMs).^{6–9} In this strategy, the Long's theory¹⁰ plays an important role, and the best results have been conquered with oblate ions in strong axial crystal fields. In particular, two SIM families have achieved the highest U_{eff} barriers and blocking temperatures: the sandwich Dy-biscyclopentadienyl complexes,^{11–13} and mononuclear pentagonal bipyramidal dysprosium compounds.^{14–16} Accordingly, the current records of blocking temperature and U_{eff} are 80 K and 2217 K,¹³ respectively. Nevertheless, there were also many failures in this field, given that a major drawback in such mononuclear systems is fast zero-field quantum tunnelling of magnetisation (QTM),¹⁷ which prevents the observation of SMM behaviour at zero field. Many strategies have been designed to constrain QTM and enhance magnetic anisotropies, among which optimising the local axial symmetry, as previously stated, or decreasing intermolecular dipolar interactions

by diluting samples,¹⁸ are efficient ways to promote functioning as SMM. Besides, such zero-field loss of magnetisation can sometimes be prevented by intramolecular interactions between spin centres, known as exchange-bias,^{19–23} although this does not necessarily ensure the elimination of the quantum tunnelling in Ln_2 complexes.²⁴ But even so, the understanding of the effect of f–f interactions and uniaxial anisotropy on the magnetic behaviour is still a challenge, and dinuclear lanthanoid complexes provide ideal models to address fundamental concerns regarding single ion behaviour *versus* properties arising from a multinuclear molecular entity.

With these considerations in mind, we describe herein the full characterisation and magnetic dynamics of dysprosium and holmium dinuclear complexes with double unsupported phenoxide bridges.

Results and discussion

Synthesis

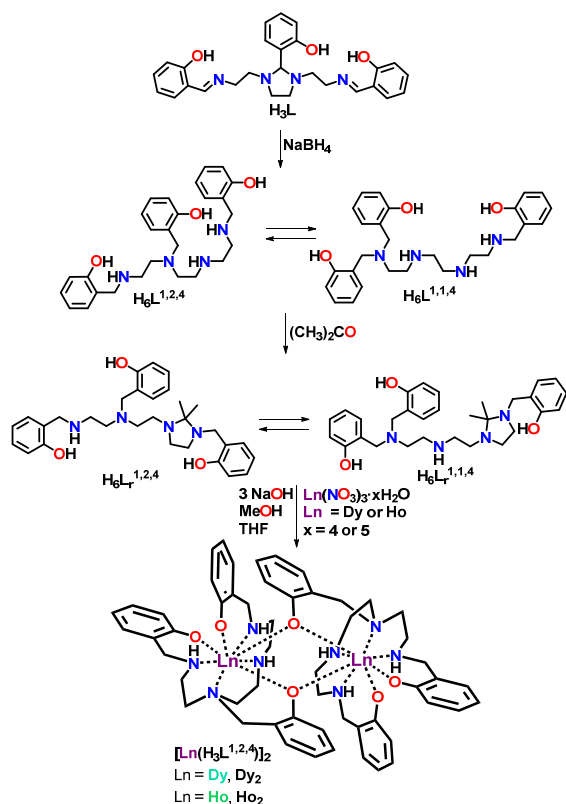
Reduction of H_3L with $NaBH_4$,²⁵ does not allow isolating a pure ligand but an oil mixture of the aminophenols $[H_6L^{1,2,4}]$ and $[H_6L^{1,1,4}]$. These are converted into the powdery ring ligands $[H_6L_r^{1,2,4}]$ and $[H_6L_r^{1,1,4}]$ by trituration with acetone, as it was previously discussed by Orvig and col.,²⁵ and by some of us,²⁶ and as it is summarised in Scheme 1. The dinuclear complexes Dy_2 and Ho_2 were isolated from the reaction of the corresponding dysprosium and holmium nitrates with this mixture of ligands (Scheme 1). These reactions give rise to the isolation of white powders, which were recrystallised in THF/MeOH. In the case of the dinuclear dysprosium complex, this recrystallisation process led to the formation of single crystals of $Dy_2 \cdot 2THF$, while for the analogous holmium compound, no single crystals suitable for X-ray diffraction studies could be obtained in this

^a Departamento de Química Inorgánica, Facultad de Química, Universidad de Santiago de Compostela, Campus Vida, 15782 Santiago de Compostela, Spain.

^b Departament de Química Inorgànica i Orgànica, and Institut de Química Teòrica i Computacional, Universitat de Barcelona, 08028 Barcelona, Spain.

^c Departamento de Química Inorgánica, Facultad de Ciencias, Universidad de Granada, Avda Fuentenueva s/n, 18071 Granada, Spain.

Electronic Supplementary Information (ESI) available: Figures S1–S9 and Tables S1–S4. CCDC. 2020902, 2020904 and 2020909. For ESI and crystallographic data in CIF format see DOI: 10.1039/x0xx00000x



Scheme 1. Reaction scheme for isolation of **Dy₂** and **Ho₂**.

way. The crystals of **Dy₂**·2THF lose the THF solvent on drying, to yield a crystalline powder of **Dy₂**, and although these single crystals allowed to study the complex by single X-ray diffraction methods, their quality was not totally satisfactory. Nevertheless, the recrystallisation of both **Dy₂** and **Ho₂** in pyridine allowed obtaining high quality single crystals of **Dy₂**·2Py and **Ho₂**·2Py, which were suitable for X-ray diffraction studies.

These three crystal structures only contain the organic ligand $[\text{H}_3\text{L}^{1,2,4}]^{3-}$ (Scheme 1). Accordingly, the initial mixture of both $[\text{H}_6\text{L}^{1,2,4}]$ and $[\text{H}_6\text{L}^{1,1,4}]$ suffers breaking of the imidazolidine ring in the presence of a metal ion, giving rise to the chain species, as awaited.²⁵⁻²⁶ In this case, the formed chain ligand is the $[\text{H}_6\text{L}^{1,2,4}]$ one, which is completely consistent with the expected results according to literature.²⁵⁻²⁶ Thus, only the crystal structures of three metal complexes with this kind of ligand have been reported up to now, one derived from $[\text{H}_6\text{L}^{1,2,4}]$ ²⁵ and two from $[\text{H}_6\text{L}^{1,1,4}]$.²⁵⁻²⁶ These studies point to the fact that the equilibrium between $[\text{H}_6\text{L}^{1,2,4}]$ and $[\text{H}_6\text{L}^{1,1,4}]$ shifts towards the $[\text{H}_6\text{L}^{1,1,4}]$ species with increasing pH of the medium. Consequently, when a nitrate salt is used as a reactant, and the NaOH base is added in 3:1 molar ratio with the ligand, as in our case study, the complex with the anionic $[\text{H}_3\text{L}^{1,2,4}]^{3-}$ donor is obtained.²⁵ However, if the base is added in 1:4 molar ratio with the ligand,²⁵ or if the basic acetate salt is employed instead of the neutral nitrate one,²⁶ the pH of the medium raises, and the compound with the $[\text{H}_3\text{L}^{1,1,4}]^{3-}$ donor is isolated. Therefore, this work contributes to strengthen the results presented in the previous scarce research dedicated to this type of donor. In addition, it must be noted that these complexes present a significant novelty, as they are the first dinuclear compounds obtained from $[\text{H}_6\text{L}^{1,1,4}]$ or $[\text{H}_6\text{L}^{1,2,4}]$ donors, given that all related complexes are mononuclear,²⁵⁻²⁶ and, therefore, they

contribute to improve the sparse coordination chemistry with these heptadentate isomers.

Dy₂ and **Ho₂** were fully characterised by analytical, spectroscopic and magnetic techniques. Crystals of **Dy₂**·2THF, **Dy₂**·2Py and **Ho₂**·2Py, obtained as described above, were studied by single crystal X-ray diffraction methods. The IR spectra of the complexes show bands at *ca.* 1560 and 1590 cm^{-1} , and about 3140 and 3270 cm^{-1} , which can be assigned to $\delta(\text{NH})$ and $\nu(\text{NH})$ vibrations,²⁷ respectively, and that agree with the protonation of non-equivalent amine groups.

X-ray diffraction studies

The crystal structures of $[\text{Dy}(\text{H}_3\text{L}^{1,2,4})]_2 \cdot 2\text{THF}$ (**Dy₂**·2THF), $[\text{Dy}(\text{H}_3\text{L}^{1,2,4})]_2 \cdot 2\text{Py}$ (**Dy₂**·2Py), and $[\text{Ho}(\text{H}_3\text{L}^{1,2,4})]_2 \cdot 2\text{Py}$ (**Ho₂**·2Py) are very similar, and they will be discussed together. The main differences among them are the different solvates (THF or pyridine), and that **Dy₂**·2THF belongs to the monoclinic space group $P2_1/n$ while **Dy₂**·2Py and **Ho₂**·2Py belong to the triclinic $P-1$ group. Ellipsoid diagrams for the complexes without solvate are shown in Figs. 1, S1 and S2, and main distances and angles are collected in Table S1.

The unit cell of the complexes contains dinuclear $[\text{M}(\text{H}_3\text{L}^{1,2,4})]_2$ ($\text{M} = \text{Dy}$ or Ho) molecules (Figs. 1, S1 and S2), and THF or pyridine as solvates. The structure of the $[\text{M}(\text{H}_3\text{L}^{1,2,4})]_2$ (**M₂**) molecules can be understood as two symmetry related neutral $[\text{M}(\text{H}_3\text{L}^{1,2,4})]$ blocks joined through two phenoxide oxygen atoms. Thus, in the $[\text{M}(\text{H}_3\text{L}^{1,2,4})]$ block, the ligand behaves as trianionic, with all the phenol oxygen atoms deprotonated, while all the secondary amine nitrogen atoms are protonated. This $[\text{H}_3\text{L}^{1,2,4}]^{3-}$ donor acts as heptadentate, using all its oxygen and nitrogen atoms to bind a M^{3+} ion. Besides, the phenoxide oxygen atom of the shortest arm of the tertiary amine of one $[\text{M}(\text{H}_3\text{L}^{1,2,4})]$ subunit (O11) binds the M^{III} centre of the second $[\text{M}(\text{H}_3\text{L}^{1,2,4})]$ subunit, and *vice versa*. Accordingly, the aminophenol ligand is acting as a heptadentate bridging ligand, a coordination mode hitherto unknown for this kind of donor, which has always been described as terminal heptadentate.²⁵⁻²⁶ This leads to symmetric M_2O_2 rhombic cycles, with $\text{M} \cdots \text{M}$ distances of *ca.* 3.94 Å and $\text{M}-\text{O}-\text{M}$ angles of *ca.* 109° (Table S1). As a result, the Ln^{III} ions in the $[\text{M}(\text{H}_3\text{L}^{1,2,4})]_2$ molecules are octacoordinated, in N_4O_4

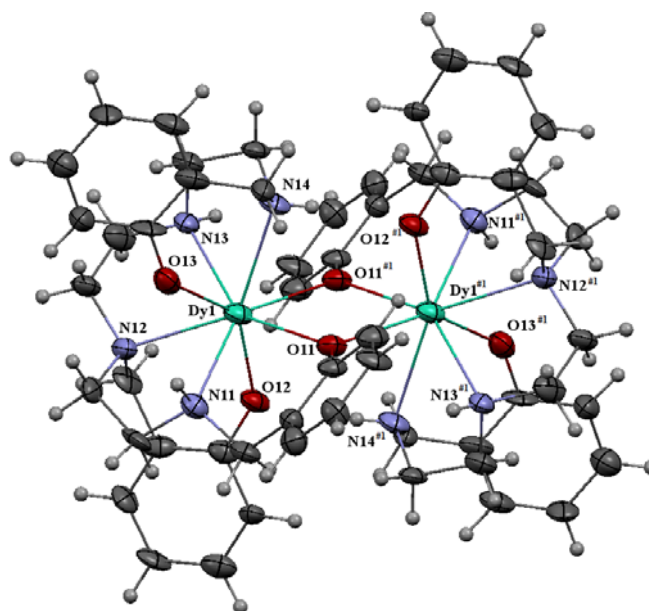


Fig. 1. Ellipsoid (50% probability) diagram for **Dy₂** (from **Dy₂**·2Py)

environments. Calculations of the distortion from ideal MN_4O_4 cores with the SHAPE program²⁸ indicate that the geometry is closer to a triangular dodecahedron, but highly distorted towards a square antiprism in all cases (Table S2). The main distances and angles about the metal ions agree with those expected for Dy^{III} or Ho^{III} complexes with polydentate N,O donors,²⁹⁻³⁰ and this aspect does not deserve much discussion. Nevertheless, it should be noted that the phenoxide bridges are non-symmetrical, and that the $M-O_{bridging}$ distances are significantly longer than the $M-O_{terminal}$ ones. In addition, it is worth mentioning that the bond distances and angles in $Dy_2 \cdot 2THF$ and $Dy_2 \cdot 2Py$ are very similar, if we take into account the standard deviations, thus suggesting that the solvates do not exert a significant influence on the geometric parameters.

Magnetic properties

Direct-current (dc) magnetic susceptibility measurements were recorded for microcrystalline samples of Dy_2 and Ho_2 as a function of the temperature. The plots of $\chi_M T$ vs T are shown in Figs. 2 and S3. The $\chi_M T$ values for Dy_2 and Ho_2 at 300 K are 27.9 and 28.5 $cm^3 K mol^{-1}$, respectively, which are very close to the expected values for two uncoupled Dy^{3+} or Ho^{3+} ions in the free-ion approximation at room temperature (28.34 $cm^3 K mol^{-1}$ for two Dy^{3+} ions, and 28.14 $cm^3 K mol^{-1}$ for two Ho^{3+} ions). The experimental curves continuously decrease until 2 K, reaching $\chi_M T$ values of 12.9 and 11.7 $cm^3 K mol^{-1}$ for Dy_2 and Ho_2 , respectively. This behaviour is mainly due to the depopulation of the M_J sublevels of the Ln^{III} ions, which arise from the splitting of the spin-orbit ground multiplet by the ligand field, as well as Zeeman effects and possible intramolecular antiferromagnetic or intermolecular dipolar interactions. These latter interactions could be responsible for the sharp decrease in $\chi_M T$ below 5 K.

The field dependence of the magnetisation at 2 K shows that the reduced magnetisation at the maximum applied field tends to 9.9 $N\mu_B$ for Dy_2 (Fig. 2, inset), and to 10.8 $N\mu_B$ for Ho_2 (Fig. S3, inset), values that are far away from the theoretical saturation value anticipated for two isolated Dy^{III} or Ho^{III} ions in the free-ion approximation (of 20 $N\mu_B$ for both cases), which is due to crystal-field effects giving rise to significant magnetic anisotropy.

The dynamic magnetic properties of Dy_2 and Ho_2 were also studied. For Dy_2 , in the absence of a dc field, both the in-phase (χ' , Fig. S4) and out-of-phase (χ'' , Fig. 3) signals of the ac susceptibility feature strong frequency-dependent phenomena, with peaks for χ'' in the temperature range 13.5–27 K. This behaviour indicates freezing of spins by a rather high thermal energy barrier to relaxation, and the quite efficient suppression of zero-field tunnelling of magnetisation

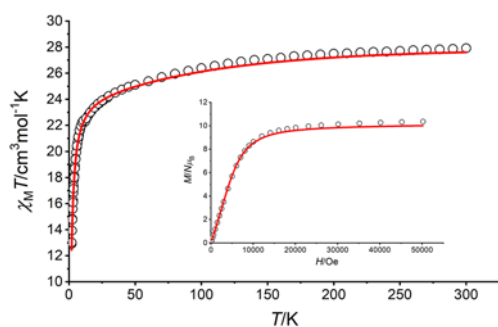


Fig. 2. $\chi_M T$ vs T for Dy_2 . Inset: $M/N\mu_B$ vs H . The solid red lines represent the theoretical data obtained from *ab initio* calculations including the dipolar interactions.

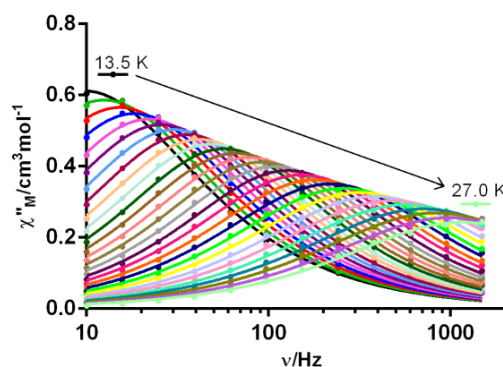


Fig. 3. Frequency dependence of χ''_M for Dy_2 in a zero dc field at different temperatures.

in this complex, which is a SMM.

Fitting the Cole–Cole plot to the generalised Debye model indicates the presence of more than one relaxation process (α parameters in the range 0.16–0.19, Fig. S5, Table S3).

The relaxation time and energy barrier for the Dy_2 SMM was extracted from the Arrhenius plot (Fig. 4). We have tried to fit this plot taking into account all the possible relaxation processes (Direct, Orbach, Raman and/or QTM), but the best fit of the curve was achieved considering Orbach and Raman relaxations processes, according to equation 1.

$$\tau^{-1} = CT^n + \tau_0^{-1} e^{-U_{eff}/k_B T} \quad (1)$$

As it can be observed in Fig. S6, the Orbach is by far the predominant relaxation process at high temperature, while the Raman process seems to govern the relaxation of the complex below 21 K. This fit yields the parameters $U_{eff} = 367.7$ K (255.5 cm^{-1}), $\tau_0 = 2.2 \times 10^{-10}$ s, $C = 4.9 \times 10^{-5} s^{-1} K^{-n}$ and $n = 5.4$. Notably, as far as we know, this is the highest energy barrier for a double-phenoxide bridged Dy_2 complex.^{24,30-31} Besides, the considerations of both the acoustic and optical phonons in magnetic dynamics cause the obtained n value deviation from the predicted value of the Kramers ion ($n = 9$).³²

The low-temperature hysteresis loop for Dy_2 was also recorded in order to test magnetic blocking, with a sweep rate of 200 Oe/s. A typical butterfly-shaped hysteresis cycle was observed in H_{dc} fields of -5–5 kOe up to 4 K (Fig. 5). However, the absence of coercivity for Dy_2 at zero field, suggests the presence of intrinsic fast QTM at low temperature, as it can also be observed in the χ''_M vs T graph by the low intensity upturn below 5 K (Fig. S7). The non-superimposed ZFC/FC curves (Fig. S8) also indicates the SMM nature of Dy_2 , in spite of the fast QTM at very low temperature.

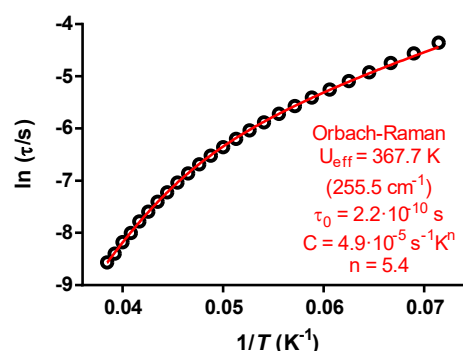


Fig. 4. Arrhenius plot for Dy_2 in zero field. The solid line accounts for the best fit considering Orbach and Raman relaxation processes.

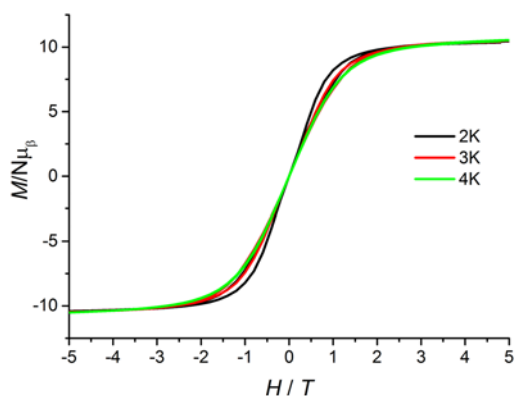


Fig. 5. Hysteresis in the $M(H)$ curve for Dy_2 , collected at temperatures ranging from 2 to 4 K with a 200 Oe/s sweep rate.

Ho_2 shows frequency dependence of the out of phase ac susceptibility in the absence of a dc magnetic field, but without reaching maxima above 2 K (Fig. 6). This means that magnetic relaxation occurs at faster frequencies than the flipping rate of the ac field above 2 K, although the complex shows quite slow relaxation of the magnetisation. The absence of SMM behaviour is probably due to a very small energy barrier and/or large quantum tunnelling of the magnetisation in this non-Kramer ion (direct QTM is due to an intrinsic tunnelling gap in the absence of applied field). Application of a static field did not change this behaviour, and the χ''_M vs ν curves also lack χ''_M peaks, but these curves are not superimposed at different magnetic fields (Fig. S9).

Although Ho_2 does not behave as a SMM, however, it constitutes a rare example of a Ho_2 complex with frequency dependence of the out of phase susceptibility. As far as we know, among dinuclear holmium complexes, only one was reported to be an SMM in the absence of a dc field at very low temperature (below 0.15 K),³³ another one was published to be a field induced SMM,³⁴ and a third one was reported to show slow relaxation of the magnetisation, but without SMM behaviour above 2 K.³⁵ Among these three compounds, two of them are phenoxide bridged complexes, with Ho_2O_2 cores.^{33,35} Accordingly, this work contributes to increase the scarce number of Ho_2 complexes with slow relaxation of the magnetisation.

Ab initio calculations

To gain more insight into the magnetic properties of the compounds reported herein, *ab initio* calculations were performed based on the single-crystal X-ray data for Dy_2Py and Ho_2Py with the software OpenMolcas³⁶ (see Computational Details). Each metal has been

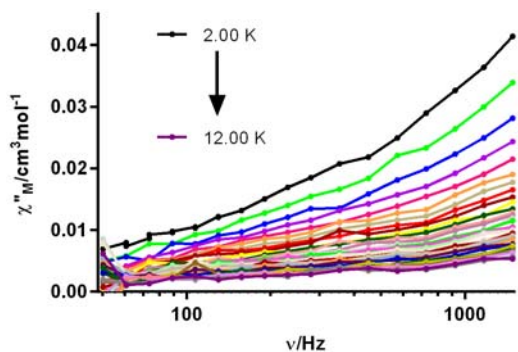


Fig. 6. Frequency dependence of χ''_M for Ho_2 in a zero-dc field at different temperatures.

Table 1. Calculated g components for the ground and first excited states at CASSCF-RASSI level for the studied systems. Two angles are shown for each compound. The first, θ , is the angle between the g_z vector and the vector connecting both metals in the dinuclear molecule. The second, γ , is the angle between the g_z vectors of the ground and first excited states.

| Compound | Dy_2 | | Ho_2 | |
|--------------|---------------|--------------------|---------------|--------------------|
| | GS | 1 st ES | GS | 1 st ES |
| g_x | 0.001 | 0.059 | 0.000 | 0.000 |
| g_y | 0.002 | 0.095 | 0.000 | 0.000 |
| g_z | 19.765 | 16.582 | 18.379 | 15.333 |
| θ (°) | 72.0 | | 83.5 | |
| γ (°) | 5.6 | | 34.3 | |

studied independently by substituting the neighbour by a close shell La^{III} ion.

For Dy_2 the calculated g -factors, collected in Table 1, show a very large axial character. The direction of the easy axis will be determined by the ligands surrounding the metal ion. The oblate shape of the electron density of the Dy^{III} centre ($^6\text{H}_{15/2}$, $M_J = 15/2$ ground state) will be accommodated between the ligands in a way that reduces the electronic repulsion. In this case each ligand is trianionic and it contributes with three phenoxide oxygen atoms. One of the phenoxide oxygen atoms of each ligand is bridging both Dy ions, while the other two phenoxide oxygen atoms of each ligand are coordinated to only one Dy^{III} ion. These latter are the ones showing the shortest Dy-O distance. The oblate electron density of the Dy^{III} centre will avoid these terminal phenolic groups and, consequently, the directions of the g_z component will be closely aligned with those Dy-O bonds, as it can be seen in Fig. 7.

The calculated lowest energy states are collected in Table S4. The first excited state is very close in energy (5.1 cm^{-1}) while the second excited state is at more than 300 cm^{-1} . It leads to a large $(E_2 - E_1)/E_1$ value, which is a figure of merit of the axiality in mononuclear Dy compounds that some of us have noticed previously.³⁷ The large difference in energy between E_2 and E_1 gives to a large axiality because the ground and first excited states, which are very close in energy, are very axial while the second excited state have less axial character, as can be seen in Figure S11.

The analysis of the energies and transition probabilities between the states after the inclusion of the spin orbit effect (Fig. 8, Table S5) shows that the tunnelling probability in the ground and first excited states is very low, which is in concordance with the low value of the transverse components of the g tensor (g_x and g_y) in Table 1. Looking at the transition probabilities, the relaxation in this case is expected

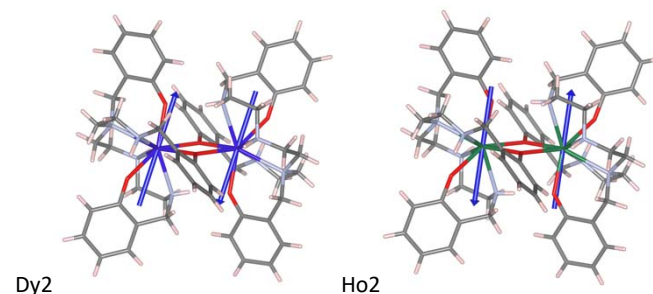


Fig. 7. Representation of the molecular structures of Dy_2 and Ho_2 showing the calculated directions of the g_z components of the Ln^{III} centres in the ground state.

to occur via the second excited state, with an energy of 342 cm^{-1} , through QTM, or via the third excited state, at 406 cm^{-1} , through an Orbach mechanism. The fact that the angle between the g_z vectors of the ground and first excited state is very small (5.6°) indicates that the relaxation does not take place through the first excited state but through higher excited states. However, the experimentally obtained energy barrier is 255.5 cm^{-1} , which is very close to the energy of the first excited state, 231.6 cm^{-1} . This can be attributed to a faster QTM in the dinuclear compound with respect to the mononuclear model, which seems favoured by the intramolecular interaction.²⁴

The interaction between both Dy^{III} centres have been also studied by means of the POLY_ANISO software and the Lines model implemented there.³⁸ The simultaneous fit of the susceptibility and magnetization curves (Fig. 2) was performed with and without including the dipolar magnetic coupling. If the magnetic dipolar coupling (J_{dipolar}) is not included, the obtained coupling constant (J) is -0.12 cm^{-1} , while if we consider the dipolar coupling, then the coupling constant value goes to -0.04 cm^{-1} . The exchange interaction leads to an energy difference of 1.4 cm^{-1} between the antiferromagnetic and ferromagnetic states. These results show the antiferromagnetic nature of the coupling, and that it is more related to the dipolar interaction than to the exchange coupling. The dipolar coupling interaction mainly depends on the magnetic moment, the distance between the magnetic centres, and the relative orientation of the magnetic moments between them. In the simplified case of two parallel interacting moments, as the one shown here, the dipolar interactions (eq. 2) depend on the angle between the magnetic moment and the vector connecting both magnetic centres. If the angle is smaller than 54.75° the interaction will be ferromagnetic while for angles larger than 54.75° an antiferromagnetic coupling will be expected. In this case study, the angle is 72° , which is in agreement with the obtained antiferromagnetic interaction.

$$E_{\text{dip}} = -\left[\frac{\mu_0}{4\pi}\right] \frac{\mu_i \mu_j}{r^3} [3\cos^2(\theta) - 1] \quad (2)$$

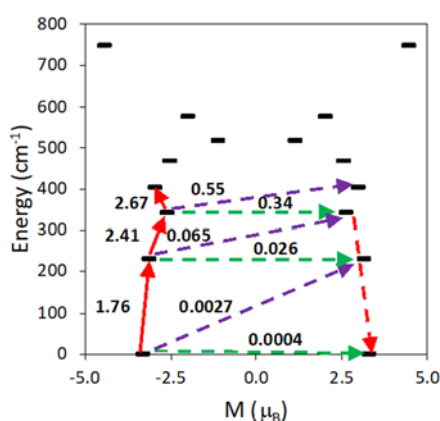


Fig. 8. States energies as a function of their average magnetic moment, M , along the main anisotropy axis for Dy_2 . The dashed green arrows correspond to the quantum tunnelling mechanism of ground or excited states, dashed purple arrow shows the hypothetical Orbach relaxation process. The solid red arrow indicates the transition between the ground and excited Kramers doublets and the dashed red arrow the excitation pathway to the ground state with the reversed spin. The values close to the arrows indicate the matrix elements of the transition magnetic moments (above 0.1 an efficient spin relaxation mechanism is expected, see Computational details).

In the case of the Ho_2 complex, the calculated lowest energy states can be described as the $^5\text{I}_8$ ground multiplets of the Ho^{III} centre. They split by the crystal field in an energy range of 400 cm^{-1} (Table S6). The g components, Table 1, show also the large axial character of the ground and excited states. However, in this case no peaks for the out of phase susceptibility are observed, probably due to the large QTM in this non-Kramer system. Nevertheless, the strong axiality could justify the slow relaxation of the magnetization.

The interaction between Ho^{III} centres have also been studied using the same procedure described for Dy_2 . When the magnetic dipolar coupling is not considered, the obtained coupling constant is -0.19 cm^{-1} , while the inclusion of the dipolar coupling gives rise to an almost negligible coupling of 0.012 cm^{-1} , and showing that in this case only the dipolar coupling is responsible and no exchange coupling is observed. The dipolar coupling in this case is larger, which is in concordance with the larger value of angle between the magnetic moment and the vector connecting both magnetic centres, 83.5° .

As a result of these calculations, it seems that the magnetic coupling between the lanthanoid centres does not destroy the quantum channel in none of the cases but, in spite of this, the bridging character of the ligand seems to be critical to the observed magnetic behaviour. Thus, the bridging coordination mode of the ligand leads to two long (*ca.* 2.34 and 2.5 \AA) and two short Ln-O (*ca.* 2.26 \AA) distances, contrary to what happens when the ligand acts as terminal heptadentate, which gives rise to compounds with three very similar Ln- O_{phenol} distances.²⁵⁻²⁶ Accordingly, the bridging character of the aminophenol donor promotes the axiality of the ground and excited states of both complexes, which seems to be responsible for their magnetic behaviour. This supposition is supported by the comparison of the structural parameters of $\text{Dy}_2\cdot 2\text{THF}$ and $\text{Dy}_2\cdot 2\text{Py}$ with those of more than 30 previously related unsupported double phenoxide bridged dinuclear dysprosium complexes.^{24,30-31} If we compare the Dy- O_{bridge} distances in our complexes (*ca.* 2.34 and 2.5 \AA) with the related ones, we can see that they are within the range of those described, as it occurs with the Dy-O-Dy bond angles and intramolecular Dy...Dy distances. Accordingly, it seems that the increased U_{eff} found in this complex is due to the elongation of Dy- O_{phenol} bridge in a complex with a donor with three oxygen atoms, what directs the anisotropy axis towards the other two short Dy-O bonds, as *ab initio* calculations demonstrates. And this appears to be the reason for the observed magnetic results, more than the value of a specific parameter or the effect of the magnetic coupling.

Conclusions

This work describes two dinuclear dysprosium and holmium complexes with a scarcely studied heptadentate aminophenol ligand, which acts in a unique bridging mode. Accordingly, they are the first dinuclear compounds obtained from $\text{H}_6\text{L}^{1,1,4}$ or $\text{H}_6\text{L}^{1,2,4}$ donors, and, therefore, this work contributes to improving the knowledge of the sparse coordination chemistry of this ligand. The magnetic properties of Dy_2 and Ho_2 are also remarkable, in such a way that the bridging character of this ligand seems to promote the axiality of the ground state and, hence, the magnetic relaxation. Thus, Dy_2 is an air stable SMM with the highest energy barrier among

dinuclear unsupported doubly phenoxide bridged dysprosium complexes, while **Ho₂** constitutes a scarcely related example of a dinuclear holmium complex with slow relaxation of the magnetisation. The magnetic results are explained in light of *ab initio* calculations, showing that the spin relaxation for the **Dy₂** system seems to occur through the second excited state. Nevertheless, the experimentally obtained energy barrier of 255.5 cm⁻¹ is smaller than the energy of the second excited state of 342 cm⁻¹. This difference between the calculated and effective energy barrier could be attributed, despite the low transition probability for the QTM in the mononuclear model, to a faster QTM in the dinuclear compound, which seems favoured by the intramolecular interactions. The dipolar or exchange intramolecular interactions are rather small, below 0.2 cm⁻¹, and they are principally dipolar in nature. The alignment of the magnetic moments are consistent with an antiferromagnetic coupling between the two metal centres for **Dy₂** and **Ho₂**. The experimental SMM behaviour found only for **Dy₂** is consistent with the Kramers nature of the Dy^{III} centres in comparison with the non-Kramers nature of the Ho^{III} cations.

Conflicts of interest

There are no conflicts to declare.

Acknowledgements

Authors thank the Spanish Ministerio de Innovación, Ciencia y Universidades (PGC2018-102052-B-C21, PGC2018-093863-B-C21 and MDM-2017-0767) for financial support. J.C.V thanks Xunta de Galicia for his Ph.D. fellowship (ED481A-2018/136). E.C. is gratefully acknowledged to the Junta de Andalucía (FQM-195 and the Project financed by FEDER funds A-FQM-172-UGR18). E.R. thanks Generalitat de Catalunya for an ICREA Academia award and for the SGR2017-1289 grant, and S.G.C. for a Beatriu de Pinòs grant. The authors acknowledge computer resources, technical expertise and assistance provided by the CSUC.

Experimental

Materials and general methods

All chemical reagents were purchased from commercial sources, and used as received without further purification. Elemental analyses of C, H and N were performed on a Carlo Erba EA 1108 analyser. Infrared spectra were recorded in the ATR mode on a Varian 670 FT/IR spectrophotometer in the range 4000–500 cm⁻¹.

Synthesis

The ligand used in this work was obtained from reduction of the previously prepared H₃L Schiff base (Scheme 1),³⁹ using a variation of a previously described method,²⁵ as formerly reported by us.²⁶ The synthetic procedure to isolate both dinuclear complexes is the same, and it is exemplified by the synthesis of [**Dy(H₃L^{1,2,4})**]₂ (**Dy₂**): To a solution of a mixture of H₆L_r^{1,1,4} and H₆L_r^{1,2,4} (0.25 g, 0.496 mmol) in THF (25 mL), NaOH (0.06 g, 1.488 mmol) and methanol (15 mL) were added. This led to a pale-yellow solution that was mixed with a previously prepared solution of Dy(NO₃)₃·6H₂O (0.226 g, 0.496 mmol)

in methanol (10 mL). The mixture was stirred at room temperature overnight (14 h), and a white solid was formed and separated by centrifugation. Recrystallisation of all the powder sample in THF/CH₃OH, and cooling the solution in the fridge, yielded small single crystals of [Dy(H₃L^{1,2,4})]₂·2THF (**Dy₂**·2THF), suitable for single X-ray diffraction studies. The crystals were collected and dried in an oven, losing the THF solvate to give rise to **Dy₂**. Yield: 0.185 g (55%). M.W.: 1248.1. Anal. calcd. for C₅₄H₆₆Dy₂N₈O₆: C 51.96, N 8.98, H 5.33 %; Found: C 51.59, N 8.83, H 5.25 %. IR (ATR, $\tilde{\nu}$ /cm⁻¹): 1564, 1592 (δ NH); 3146, 3271 (ν NH).

Recrystallisation of a small portion of the microcrystalline solid in pyridine/methanol yielded single crystals of [Dy(H₃L^{1,2,4})]₂·2Py (**Dy₂**·2Py), also suitable for X-ray diffraction studies.

[**Ho(H₃L^{1,2,4})**]₂ (**Ho₂**): amounts of impure ligand (0.25 g, 0.496 mmol), NaOH (0.06 g, 1.488 mmol) and Ho(NO₃)₃·5H₂O (0.219 g, 0.496 mmol). The complex was obtained in the form of a white powder. Yield: 0.1 g (30%). M.W.: 1252.98. Anal. calcd. for C₅₄H₆₆Ho₂N₈O₆: C 51.76, N 8.94, H 5.31 %; Found: C 51.65, N 8.93, H 5.20 %. IR (ATR, $\tilde{\nu}$ /cm⁻¹): 1564, 1593 (δ NH); 3142, 3272 (ν NH).

Recrystallisation of the white solid in pyridine/methanol yielded single crystals of [Ho(H₃L^{1,2,4})]₂·2Py (**Ho₂**·2Py), suitable for X-ray diffraction studies.

X-ray diffraction studies

Crystal data and details of refinement are given in Table S7. The single crystals of **Dy₂**·2THF, **Dy₂**·2Py and **Ho₂**·2Py could be obtained as detailed above. Data were collected at 100 K on a Bruker D8 VENTURE PHOTON III-14 diffractometer, employing graphite monochromatised Mo-K α (λ = 0.71073 Å) radiation. Multi-scan absorption corrections were applied using the SADABS routine.⁴⁰ The structures were solved by standard direct methods employing SHELXT,⁴¹ and then refined by full matrix least-squares techniques on F^2 by using SHELXL, from the program package SHELX-2018.⁴¹ As a general method, all atoms different from hydrogen were anisotropically refined, while H atoms were typically included in the structure factor calculations in geometrically idealised positions. However, with the intention of revealing the hydrogen bonding scheme, hydrogen atoms attached to amine nitrogen atoms were located in the corresponding Fourier map. In this case, either they were freely refined, or with thermal parameters derived from their parent atoms.

It must be mentioned that crystals of **Dy₂**·2THF presented enough quality to be solved, but their refinement was not fully satisfactory, and the resulting crystal structure presents too high calculated residual densities which cannot be sensibly assigned to atoms, being the highest one 5.92 eÅ⁻³ at 0.87 Å from Dy1, while the lowest one (-2.91 eÅ⁻³) is at 1.06 Å from C108. Owing to this and other problems, the compound was recrystallised in pyridine to avoid these inconveniences and in order to use more accurate crystal results for *ab initio* calculations.

Magnetic measurements

Magnetic susceptibility dc and ac measurements for a microcrystalline sample of **Dy₂** were carried out with a Quantum Design SQUID MPMS-XL susceptometer, and those of **Ho₂** and the hysteresis measurements for **Dy₂** with a PPMS Quantum Design susceptometer. The dc magnetic susceptibility data were recorded

under a magnetic field of 3000 Oe in the range 2-300 K. Magnetisation measurements at 2.0 K were recorded under magnetic fields ranging from 0 to 50000 Oe or to 70000 Oe for Dy_2 and Ho_2 , respectively. Diamagnetic corrections were estimated from Pascal's Tables. Alternating current (ac) susceptibility measurements at zero dc field were performed with an oscillating ac field of 3.5 Oe (Dy_2) or 10 Oe (Ho_2) and ac frequencies ranging from 10 to 1500 Hz. For Ho_2 , alternating current (ac) susceptibility measurements were also recorded at 2.5 K at different fields ranging from 0 to 2000 Oe, and ac frequencies ranging from 50 to 1700 Hz.

Computational details

Multireference calculations were performed using OpenMolcas software⁴² based on the single-crystal X-ray data for $\text{Dy}_2\cdot\text{Py}$ and $\text{Ho}_2\cdot\text{Py}$. The data for $\text{Dy}_2\cdot\text{Py}$ were chosen and not those of $\text{Dy}_2\cdot 2\text{THF}$ because the crystallographic data for the former are better. For each compound, each metal has been studied independently by using the fragment approach, one of the metals was substituted by the close shell La^{3+} ion. Due to the symmetry of the molecules the results for each metal were identical and only the data for one of them is showed.

The state energies without spin-orbit effects were calculated using the CASSCF method and the spin-orbit coupling was included perturbatively in a second step by using the restricted active space state interaction method (RASSI).⁴³ For the studied type of compounds the large ionic character of the Ln-O/N bonds makes unnecessary the inclusion of the dynamic correlation contributions. The MOLCAS ANO-RCC basis set³⁶ was used for all the atoms, which the following contractions: Ho [9s8p6d4f3g2h], Dy [9s8p6d4f3g2h], La [9s8p6d4f3g2h], O [4s3p2d1f], N [4s3p2d1f], C [3s2p] and H [2s]. For the Dy and Ho compounds a (9,7) and (10,7) active spaces were employed respectively. For Dy 21 sextets, 128 quadruplets and 98 doublets were considered, while for Ho 35 quintuplets, 57 triplets and 55 singlets were included. The Single_Aniso routine, as implemented in OpenMolcas, was employed to evaluate the magnetic properties of the individual fragments and the simulation of the anisotropic exchange interactions was performed with the Poly_Aniso program.³⁸ To have an estimation of the probability of transition between two different states of the molecules the matrix elements of the transition magnetic moments have been calculated as proposed by the golden Fermi rule, as the integral between the two involved states using a magnetic moment operator.⁴⁴

References

- R. Sessoli and A. K. Powell, Strategies towards single molecule magnets based on lanthanide ions, *Coord. Chem. Rev.*, 2009, **253**, 2328-2341.
- L. Sorace, C. Benelli and D. Gatteschi, Lanthanides in molecular magnetism: old tools in a new field, *Coord. Chem. Rev.*, 2011, **40**, 3092-3104
- D. N. Woodruff, R. E. P. Winpenny and R. A. Layfield, Lanthanide single-molecule magnets, *Chem. Rev.*, 2013, **113**, 5110-5148.
- J. Tang and P. Zhang, *Lanthanide single molecule magnets*, Springer-Verlag GmbH, Berlin, 2015.
- S. T. Liddle and J. van Slageren, Improving f-element single molecule magnets, *Chem. Soc. Rev.*, 2015, **44**, 6655–6669.
- S. K. Gupta and R. Murugavel, Enriching lanthanide single-ion magnetism through symmetry and axiality, *Chem. Commun.*, 2018, **54**, 3685-3696.
- (a) A. K. Bar, P. Kalita, M. K. Singh, G. Rajaraman and 2018, 367, 163–216. (b) A. Dey, P. Kalita and V. Chandrasekhar, Lanthanide(III)-based single-ion magnets, *ACS Omega*, 2018, **3**, 9462–9475.
- Z. Zhu, M. Guo, X.-L. Li and J. Tang, Molecular magnetism of lanthanide: Advances and perspectives, *Coord. Chem. Rev.* 2019, **378**, 350–364
- J.-H. Jia, Q.-W. Li, Y.-C. Chen, J.-L. Liu and M.-L. Tong, Luminescent single-molecule magnets based on lanthanides: design strategies, recent advances and magneto-luminescent studies, *Coord. Chem. Rev.*, 2019, **378**, 365–381.
- J. D. Rinehart and J. R. Long, Exploiting single-ion anisotropy in the design of f element single-molecule magnets, *Chem. Sci.*, 2011, **2**, 2078–2085.
- a) F.-S. Guo, B. M. Day, Y.-C. Chen, M.-L. Tong, A. Mansikkamäki and R. A. Layfield, A dysprosium metallocene single-molecule magnet functioning at the axial limit, *Angew. Chem. Int. Ed.*, 2017, **56**, 11445–11449. (b) C. A. P. Goodwin, F. Ortu, D. Reta, N. F. Chilton and D. P. Mills, Molecular magnetic hysteresis at 60 kelvin in dysprosocenium. *Nature*, 2017, **548**, 439–442.
- K. R. McClain, C. A. Gould, K. Chakarawet, J. S. Teat, T. J. Groshens, J. R. Long and B. G. Harvey High-temperature magnetic blocking and magneto-structural correlations in a series of dysprosium(III) metallocenium single-molecule magnets *Chem. Sci.*, 2018, **9**, 8492-8503.
- F.-S. Guo, B. M. Day, Y.-C. Chen, M.-L. Tong, A. Mansikkamäki and R. A. Layfield, Magnetic hysteresis up to 80 kelvin in a dysprosium metallocene single-molecule magnet, *Science*, 2018, **362**, 1400-1403.
- Y.-C. Chen, J.-L. Liu, L. Ungur, J. Liu, Q.-W. Li, L.-F. Wang, Z.-P. Ni, L. F. Chibotaru, X.-M. Chen and M.-L. Tong, Symmetry-supported magnetic blocking at 20 K in pentagonal bipyramidal Dy(III) single-ion magnets, *J. Am. Chem. Soc.* **2016**, **138**, 2829-2837.
- L. Zhu, B. Yin, P. Ma and D. Li, Tuning the equatorial crystal-field in mononuclear Dy^{III} complexes to improve single-molecule magnetic properties. *Inorg. Chem.*, 2020, **59**, 16117–16121.
- Y.-S. Ding, N. F. Chilton, R. E. P. Winpenny and Y.-Z. Zheng, On approaching the limit of molecular magnetic anisotropy: a near-perfect pentagonal bipyramidal dysprosium(III) single-molecule magnet. *Angew. Chem., Int. Ed.*, 2016, **55**, 16071-16074.
- N. Ishikawa, M. Sugita and W. Wernsdorfer, Quantum tunneling of magnetization in lanthanide single-molecule magnets: bis(phthalocyaninato)terbium and bis(phthalocyaninato)dysprosium anions, *Angew. Chem., Int. Ed.*, 2005, **44**, 2931–2935.
- K. R. Meihaus, J. D Rinehart and J. R. Long, Dilution-induced slow magnetic relaxation and anomalous hysteresis in trigonal

- prismatic dysprosium(III) and uranium(III) complexes, *Inorg. Chem.*, 2011, **50**, 8484-8489.
- 19 S. Sakaue, A. Fuyuhira, T. Fukuda and N. Ishikawa, Dinuclear single-molecule magnets with porphyrin-phthalocyanine mixed triple-decker ligand systems giving SAP and SP coordination polyhedral, *Chem. Commun.*, 2012, **48**, 5337-5339.
 - 20 J. Long, F. Habib, P.-H. Lin, I. Korobkov, G. Enright, L. Ungur, W. Wernsdorfer, L. F. Chibotaru and M. Murugesu, Single-molecule magnet behavior for an antiferromagnetically superexchange-coupled dinuclear dysprosium(III) complex, *J. Am. Chem. Soc.*, 2011, **133**, 5319-5328.
 - 21 S. Demir, M. I. Gonzalez, L. E. Darago, W. J. Evans and J. R. Long, Giant coercivity and high magnetic blocking temperatures for N_2^{3-} radical-bridged dilanthanide complexes upon ligand dissociation, *Nat. Commun.*, 2017, **8**, 2144.
 - 22 J. Xiong, H.-Y. Ding, Y.-S. Meng, C. Gao, X.-J. Zhang, Z.-S. Meng, Y.-Q. Zhang, W. Shi, B.-W. Wang and S. Gao, Hydroxide-bridged five-coordinate Dy III single-molecule magnet exhibiting the record thermal relaxation barrier of magnetization among lanthanide-only dimers, *Chem. Sci.*, 2017, **8**, 1288-1294.
 - 23 L. Zhang, J. Jung, P. Zhang, M. Guo, L. Zhao, J. Tang and B. Le Guennic, Site-resolved two-step relaxation process in an asymmetric Dy_2 single-molecule magnet, *Chem. Eur. J.*, 2016, **22**, 1392 – 1398.
 - 24 H.-M. Dong, H.-Y. Li, Y.-Q. Zhang, E.-C. Yang and X.-J. Zhao, Magnetic relaxation dynamics of a centrosymmetric Dy_2 single-molecule magnet triggered by magnetic-site dilution and external magnetic field, *Inorg. Chem.*, 2017, **56**, 5611–5622, and references therein.
 - 25 L.-W. Yang, S. Liu, E. Wong, S. J. Rettig and C. Orvig, Complexes of trivalent metal ions with potentially heptadentate N_4O_3 Schiff base and amine phenol ligands of varying rigidity, *Inorg. Chem.*, 1995, **34**, 2164-2178.
 - 26 M. Fondo, J. Corredoira-Vázquez, A. M. García-Deibe, J. Sanmartín-Matalobos, M. Amoa, A. M. P. Botas, R. A. S. Ferreira, L. D. Carlos and E. Colacio, Field-induced slow magnetic relaxation and luminescence thermometry in a mononuclear ytterbium complex, *Inorg. Chem. Front.*, 2020, **7**, 3019-3029.
 - 27 K. Nakamoto, *Infrared and Raman Spectra of Inorganic and Coordination Compounds*, Ed. John Wiley & Sons, New York, 1997.
 - 28 (a) M. Llunell, D. Casanova, J. Cirera, J. M. Bofill, P. Alemany, S. Alvarez, M. Pinsky and D. D. Avnir, SHAPE v1.1b, Barcelona, 2005; (b) A. Ruiz-Martínez, D. Casanova and S. Alvarez, Polyhedral structures with an odd number of vertices: nine-coordinate metal compounds, *Chem. Eur. J.*, 2008, **14**, 1291–1303; (c) M. Llunell, D. Casanova, J. Cirera, P. Alemany and S. Alvarez, SHAPE: Program for the stereochemical analysis of molecular fragments by means of continuous shape measures and associated tools; University of Barcelona, Barcelona, Spain, 2010.
 - 29 (a) M. Fondo, J. Corredoira-Vázquez, A. M. García-Deibe, J. Sanmartín-Matalobos, J. M. Herrera and E. Colacio, Tb_2 , Dy_2 , and Zn_2Dy_4 complexes showing the unusual versatility of a hydrazone ligand toward lanthanoid ions: a structural and magnetic study, *Inorg. Chem.*, 2018, **57**, 10100–10110; (b) M. Fondo, J. Corredoira-Vázquez, A. M. García-Deibe, S. Gómez-Coca, E. Ruiz and J. Sanmartín-Matalobos, Dysprosium-based complexes with a flat pentadentate donor: a magnetic and *ab initio* study, *Dalton Trans.*, 2020, **49**, 8389-8401.
 - 30 H.-H. Chen, D.-F. Wu, Y.-Y. Duan, L. Li, Y.-J. Wang, X.-M. Zhang, J.-Z. Cui and H.-L. Gao, The near-infrared luminescence and magnetism of dinuclear complexes with different local symmetries constructed from a β -diketonate co-ligand and bis-Schiff base ligand, *New J. Chem.*, 2020, **44**, 2561-2570.
 - 31 S. Liu, J. Lu, X.-L. Li, Z. Zhua and J. Tang, Counter anions influence the relaxation dynamics of phenoxy-bridged Dy_2 single molecule magnets, *Dalton Trans.*, 2020, **49**, 12372–12379.
 - 32 (a) A. Singh and K. N. Shrivastava, Optical-acoustic two-phonon relaxation in spin systems, *Phys. Status Solidi B*, 1979, **95**, 273-277; (b) K. N. Shrivastava, Theory of spin–lattice relaxation, *Phys. Status Solidi B*, 1983, **117**, 437-458.
 - 33 M. Viciano-Chumillas, F. Koprowiak, I. Mutikainen, W. Wernsdorfer, T. Mallah and H. Bolvin, Hysteresis in a bimetallic holmium complex: a synergy between electronic and nuclear magnetic interactions, *Phys. Rev. B*, 2017, **96**, 214427.
 - 34 J. D. Rinehart, M. Fang, W. J. Evans and J. R. Long, A N_2^{3-} radical-bridged terbium complex exhibiting magnetic hysteresis at 14 K, *J. Am. Chem. Soc.*, 2011, **133**, 14236-1239.
 - 35 J. Zhang, H. Zhang, Y. Chen, X. Zhang, Y. Li, W. Liu and Y. Dong, A series of dinuclear lanthanide complexes with slow magnetic relaxation for Dy_2 and Ho_2 , *Dalton Trans.*, 2016, **45**, 16463–16470.
 - 36 (a) B. O. Roos, R. Lindh, P.-Å. Malmqvist, V. Veryazov, P.-O. Widmark and A. C. Borin, New relativistic atomic natural orbital basis sets for lanthanide atoms with applications to the Ce diatom and LuF_3 , *J. Phys. Chem. A*, 2008, **112**, 11431–11435; (b) B. O. Roos, R. Lindh, P. Å. Malmqvist, V. Veryazov and P.-O. Widmark, Main group atoms and dimers studied with a new relativistic ANO basis set, *J. Phys. Chem. A*, 2004, **108**, 2851–2858; (c) P.-O. Widmark, P.-Å. Malmqvist and B. O. Roos, Density matrix averaged atomic natural orbital (ANO) basis sets for correlated molecular wave functions, *Theor. Chim. Acta*, 1990, **77**, 291–306.
 - 37 (a) D. Aravena and E. Ruiz, Shedding light on the single-molecule magnet behavior of mononuclear Dy^{III} complexes. *Inorg. Chem.*, 2013, **52**, 13770– 13778; (b) S. Gomez-Coca, D. Aravena, R. Morales and E. Ruiz, Large magnetic anisotropy in mononuclear metal complexes. *Coord. Chem. Rev.*, 2015, **289**, 379–392.
 - 38 (a) L. Ungur, W. Van den Heuvela and L. F. Chibotaru, Ab initio investigation of the non-collinear magnetic structure and the lowest magnetic excitations in dysprosium triangles. *New J. Chem.*, 2009, **33**, 1224-1230; (b) L. F. Chibotaru, L. Ungur, and A. Soncini, The origin of nonmagnetic Kramers doublets in the ground State of dysprosium triangles: evidence for a toroidal magnetic moment. *Angew. Chem. Int. Ed.*, 2008, **47**, 4126-4129; (c) L. F. Chibotaru, L. Ungur, C. Aronica, H. Elmoll, G. Pilet and D. Luneau, Structure, magnetism, and theoretical study of

- a mixed-valence $\text{Co}^{\text{II}}_3\text{Co}^{\text{III}}_4$ heptanuclear wheel: lack of SMM behavior despite negative magnetic anisotropy. *J. Am. Chem. Soc.*, 2008, **130**, 12445–12455.
- 39 M. Fondo, A. M. García-Deibe, M. R. Bermejo, J. Sanmartín and A. L. Llamas-Saiz, Spontaneous carbon dioxide fixation: a μ_4 -carbonate bridged tetranuclear zinc(II) complex of a heptadentate Schiff base *J. Chem. Soc., Dalton Trans.*, 2002, 4746–4750.
- 40 G. M. Sheldrick, *SADABS, Area-Detector Absorption Correction*; Siemens Industrial Automation, Inc.: Madison, WI, 2001.
- 41 G. M. Sheldrick, Crystal structure refinement with SHELXL. *Acta Cryst.*, 2015, **C71**, 3–8.
- 42 I. Fdez. Galván, M. Vacher, A. Alavi, C. Angeli, F. Aquilante, J. Autschbach, J.J. Bao, S.I. Bokarev, N.A. Bogdanov, R.K. Carlson, L.F. Chibotaru, J. Creutzberg, N. Dattani, M.G. Delcey, S.S. Dong, A. Dreuw, L. Freitag, L.M. Frutos, L. Gagliardi, F. Gendron, A. Giussani, L. González, G. Grell, M. Guo, C.E. Hoyer, M. Johansson, S. Keller, S. Knecht, G. Kovačević, E. Källman, G. Li Manni, M. Lundberg, Y. Ma, S. Mai, J.P. Malhado, P.Å. Malmqvist, P. Marquetand, S.A. Mewes, J. Norell, M. Olivucci, M. Oppel, Q.M. Phung, K. Pierloot, F. Plasser, M. Reiher, A.M. Sand, I. Schapiro, P. Sharma, C.J. Stein, L.K. Sørensen, D.G. Truhlar, M. Ugandi, L. Ungur, A. Valentini, S. Vancoillie, V. Veryazov, O. Weser, T.A. Wesółowski, P.-O. Widmark, S. Wouters, A. Zech, J.P. Zobel, R. Lindh, OpenMolcas: From Source Code to Insight, *J. Chem. Theory Comput.*, 2009, **15**, 5925–5964.
- 43 P. Å. Malmqvist, B. O. Roos and B. Schimmelpfennig, The restricted active space (RAS) state interaction approach with spin-orbit coupling, *Chem. Phys. Lett.*, 2002, **357**, 230–240.
- 44 L. Ungur and L. Chibotaru, Strategies toward high-temperature lanthanide-based single-molecule magnets, *Inorg. Chem.*, 2016, **556**, 10043–10056.